Combust. Sci. and Tech., 182: 858–878, 2010

ISSN: 0010-2202 print/1563-521X online
DOI: 10.1080/00102200903401241

Taylor & Francis
Taylor & Francis Group

FLUID DYNAMIC STRUCTURES IN A FIRE ENVIRONMENT OBSERVED IN LABORATORY-SCALE EXPERIMENTS

Jesse Lozano,[1] Watcharapong Tachajapong,[1] David R. Weise,[2] Shankar Mahalingam,[1] and Marko Princevac[1]
[1]*Department of Mechanical Engineering, University of California Riverside, Riverside, CA, USA*
[2]*USDA Forest Service, Pacific Southwest Research Station, Riverside, CA, USA*

Particle Image Velocimetry (PIV) measurements were performed in laboratory-scale experimental fires spreading across horizontal fuel beds composed of aspen (Populus tremuloides Michx) excelsior. The continuous flame, intermittent flame, and thermal plume regions of a fire were investigated. Utilizing a PIV system, instantaneous velocity fields for the three regions were measured and special attention was given to the coherent fluid dynamic structures that are present in a propagating fire environment. Measurements were performed inside the fire itself and in the surrounding environment. From the PIV data the formation of vortex structures in front of the fire were observed. For the 3 flame regions, instantaneous velocity field data was analyzed to determine existing vortex diameters and vorticity values. The presented results of the detailed and measured velocity field within a propagating fire are likely the first of its type.

Keywords: Firespread; Particle image velocimetry; Vorticity

1. INTRODUCTION

Wildland fires have been viewed both as a natural phenomenon that helps maintain ecological balance and as a source of threat to humans and property. Fire spread rate is strongly dependent on the nature of the fuel and environmental conditions. Fuel depths range from a few millimeters in deserts to a few meters in shrubs and organic soils to tens of meters in coniferous and eucalyptus tree crowns. Ground fires occurring in accumulated, decomposed organic materials can have spread rates of the order of cm/hr (Frandsen, 1991). Surface fires involve loose dead fuels on the forest floor or grasses in open land. Surface fires in loose dead forest fuels travel at rates of 100–200 m/hr whereas wind-driven fires in grass and shrublands may travel at rates of 15–20 km/hr (Pyne et al., 1996). Crown fires occur in extensive brush fields in Mediterranean regions of the world, in dense coniferous forests in northern

Received 22 April 2009; revised 28 August 2009; accepted 9 October 2009.
Address correspondence to Jesse Lozano, Bourns Hall B242, Department of Mechanical Engineering, University of California Riverside, Riverside, CA 92521, USA. E-mail: lozanj02@student.ucr.edu

temperate and boreal regions, and in eucalyptus forests in Australia. Large surface fires and crown fires are typically the most damaging fires to life, property, and natural resources. Many different mathematical models have been developed to predict different aspects of wildland fire behavior to aid managers charged with protecting people, property, and natural resources from wildfires and managers who use wildland fire to accomplish natural resource management objectives. These models are designed to predict the evolution of a fire as a function of fuel properties, mean wind speed and direction, and terrain topography. The merits and assumptions of the various models have been reviewed previously and the interested reader is encouraged to examine these reviews (Catchpole and de Mestre, 1986; Pastor et al., 2003; Pitts, 1991; Weber, 1991). Present operational fire models such as BEHAVE (Andrews, 1986), FARSITE (Finney, 1998) and BRNPLN (Hilbruner, 1988) are computer implementations of the Rothermel spread model (Rothermel, 1972). Another implementation of the Rothermel model in southern California called FIRECAST (Cohen, 1986) added chaparral fuel beds based on Rothermel and Philpot's (1973) work. These models make various simplified fuel parameter assumptions that are inconsistent with field observations (Andrews and Queen, 2001; Ottmar et al., 2007; Parsons, 2006). Rothermel's model assumes uniform fuel, dominated by dead material close to the ground, and constant environmental conditions. The heat transfer mechanisms were not explicitly described. It was observed (Carrier et al., 1991; Viegas, 2004; Wolff et al., 1991; Zhou et al., 2005) that under wind-aided conditions, convective energy transfer plays a more prominent role in the ignition of unburned fuel in contrast to no wind conditions where radiation dominates. In order to estimate the convective energy transfer, it is necessary to characterize the buoyant plume, namely its dimensions, temperature, and air velocity distribution (Cruz, 2006). Predicting fire behavior is also highly dependent on knowledge of fuel characteristics (Countryman and Philpot, 1970). Fire spread within wildland fuels is maintained by thermal energy release from fuel combustion, flame and ember radiation heat transfer, convective heat transfer, and through advection effects such as rolling embers and spotting (Sun, 2006). Rolling embers from wildland fires promote spotting, which can ignite large fires at various distances from the source fire. It was observed that conifer needles, pollen cones, cone scales, bracts, and wood fragments were transported by wind and subsequently deposited up to 20 km from a forest fire (Pisaric, 2002). Present operational models do not include a two-way coupling between the fire and the atmosphere. Research or physical models of fire behavior, on the other hand, focus on improved methodologies and are often limited in scope and designed to better understand specific physical processes. The earliest coupled atmosphere-fire research model is due to Grishin (1992). Since then, Clark et al. (1996), Linn et al. (2002), and Mell et al. (2007) also developed such coupled models and applied them to relatively large scales, with the smallest, unresolved length scales ranging from 1 to 10 m.

To validate existing physical models for fire behavior, it is important to perform experiments and collect data that can be compared to model predictions. Although data exists that describes fire spread rate and some qualitative aspects of wildfire behavior, little data has explicitly revealed the small time and spatial scales in the convective processes that may determine the rate of fire spread (Clark et al., 1999). Fire spread studies in wooden cribs found that convective heating accounted for over 50% of the total energy budget (McCarter and Broido, 1965). In fuel beds of pine needle litter, Anderson (1969) reported that 40% of total heat transfer was accounted for by radiant heat transfer and concluded that convective heat transfer at the interface of the combustion zone and the unburned fuel probably accounts for the rest. Recent modeling of marginal fire spread in live fuel beds has also suggested the importance of convective heating (Zhou et al., 2007).

Wind flow measurements in the vicinity of large fires have been performed in field settings using anemometers and other devices (Clements et al., 2008; Meroney, 2007; Pitts, 1991; Taylor et al., 2004). Although researchers have measured instantaneous two-dimensional (2D) velocity fields in turbulent flows involving combustion (Bryant, 2005, 2009a, 2009b; Long et al., 2006; Reuss et al., 1990; Sun et al., 2006; Zhou and Garner, 1995), with the exception of the recent work by Clements et al. (2008), we are unaware of measurement of instantaneous velocity fields within a spreading fire. Reuss et al. (1990) used a Particle Image Velocimetry (PIV) system to obtain the instantaneous velocity field over a 24 mm × 32 mm area in a two-stroke engine. From the PIV data they were able to resolve the velocity integral-length scales. Zhou and Garner (1995) used a PIV system to investigate flame propagation and unburned gas velocity fields within a cylindrical combustion chamber. Through use of the PIV system they were able to determine the local flame speed. Long et al. (2006) utilized a PIV system to examine how flame fronts interact with simple toroidal vortex structures in a controlled environment. The PIV allowed them to investigate how the toroidal vortices distorted the flame front, and how this in turn affected the progression of the flame. In their study, Long et al. (2006) used a 138 mm × 108 mm imaging area. Three vortex sizes each resulting from air being pushed through different orifice sizes 40, 30, and 20 mm, by a progressing flame front, were investigated. From their analysis, Long et al. (2006) determined that there were three distinct modes of flame-vortex interaction: (a) the flame propagates around the vortex following the streamlines, pushing the vortex ahead of the flame and slowly consuming the mixture in the vortex (orifice size of 40 mm); (b) the flame initially propagates around the vortex and then rapidly consumes the vortex (orifice size of 30 mm); and (c) the flame immediately and rapidly consumes the mixture in the vortex (orifice size 20 mm). Sun et al. (2006) performed experiments on chaparral fuels and used a Thermal Particle Image Velocity (TPIV) method to estimate the flow velocities in the vicinity of a flame utilizing an IR camera. The TPIV method traces thermal particles. across successive IR images to determine the instantaneous velocity field. In TPIV, the thermal particles are virtual particles that correspond to pixels of temperature values resolved in IR images, and it is assumed that these particles rotate and translate, behaving like fluid particles. Bryant (2005) used a Stereoscopic PIV (SPIV) system to measure the velocity of a buoyancy-induced flow through a doorway and to compare gas velocity measurements in a full-scale enclosure fire (Bryant, 2009a, 2009b). In the SPIV system a second camera is introduced into the image capturing setup to view the same area as the first camera but from a different angle, and this allows the out of plane displacement of the particles to be determined. The velocity components are then calculated by dividing the resulting displacement components by the time interval between each laser pulse, as with traditional PIV. Bryant (2009a, 2009b) performed a study in which the velocity measurements taken using the SPIV system were compared to the velocity measurements recorded using a series of vertically placed bidirectional probes based on the design by McCaffrey and Heskestad (1967). The flow measured in this study resulted from a fire contained within an enclosure. Air flow was induced into the enclosure due to the buoyancy of the hot products of combustion from the fire exiting the room. As the hot products of combustion exited the enclosure, air from the outside of the enclosure was entrained into the enclosure resulting in a region where the flow moved in opposite directions (flow interface). Bryant (2009a, 2009b) reported that the velocity measured from the bidirectional probe was on average 7% greater than that determined from the SPIV system. In addition to the challenges associated with making measurements in a flow field involving high heat release, a spreading fire poses additional challenges. First, the region of interest (i.e., the fire front) evolves with time as the fire spreads spatially, and second, it is nontrivial to introduce seed particles required to make velocity measurements into the region of interest. Since to our knowledge the presented results of the detailed velocity field within a propagating fire are likely the first of its type, it is important to ensure that it is possible to successfully seed a propagating fire to attain velocity field data both in the vicinity of the fire and within the fire itself. Hence, a simple configuration in which a surface fire spreads under no wind conditions was selected for detailed investigation. This limits the resulting fire intensity, defined as the energy released per unit length of a fire line. Such a situation results in a marginal burning condition that is relevant for prescribed fires (Weise et al., 2005). Furthermore, the elimination of imposed ambient wind results in a fire spread condition dominated by radiant preheating of the fuel ahead of the front (Rothermel, 1983).

In this paper, a laboratory approach that directly addresses the small temporal and spatial scales associated with convective processes within and around a surface fire, is presented and discussed. A PIV system is used to measure 2D instantaneous velocity field in the vicinity and within a propagating fire front for no-wind conditions. The three fire regions, (a) continuous flame, (b) intermittent flame, and (c) thermal plume, are investigated to determine the various fluid dynamic structures that are present in a propagating fire environment at laboratory scale. There are various definitions to describe the boundaries of the three regions. Zukoski (1995) defined the continuous flame region as the part of the flame in which combustion continuously produces heat addition as a result of ongoing chemical reactions, the intermittent flame region as the unsteady region in which flaming combustion is intermittent, and the far field region (thermal plume region) as the region above the flame in which chemical reactions are very slow and a buoyant plume is formed. McCaffrey (1979) defined the continuous flame region as the part of the flame where ΔT (temperature rise above ambient), remains nearly constant and as starting from the surface of the fuel source with vertical velocity, V equal to zero, at the surface, and rising with the height above the fuel source z, to the $1/2$ power. The intermittent flame region is defined as having nearly constant V and where ΔT decreases with height to the first power, and the thermal plume region as being free of flames with $V \sim z^{-1/3}$ and $\Delta T \sim z^{-5/3}$. The three flame regions in this study are defined as the following: continuous flame region, located in the lower part of the fire plume, from the surface of the fuel to the minimum flame height as determined through video images, where the hot gas temperature is relatively constant (McCaffrey, 1979); intermittent flame region, from the minimum to the maximum flame height, where flame oscillation is observed and the hot gas flame temperature decreases with height; thermal plume region, beyond the maximum flame height where no more flames are visible and hot gas temperatures continue to decrease with height.

2. METHODS

2.1. Experimental Technique

A PIV system was utilized to measure the instantaneous velocity field in a vertical plane within a propagating surface fire. Independent measurement methods were not used to determine the accuracy of the PIV velocity measurements. However, other researchers, such as Bryant (2005, 2009a, 2009b), have determined the accuracy of the PIV method to be satisfactory, although it is noted that their measurements were in relatively lower temperature regions away from a direct fire. The PIV technique measures the velocity in a fluid by correlating images of the particle-seeded flow (Adrian, 1988). For these experiments, approximately 70 g per experiment of aluminum oxide (Al_2O_3) was utilized as the seeding particles. The particle size range is from 10 to 44 mm and particle density is 3970 kg/m^3. These particles were chosen because they are readily available at low cost and, most importantly, are able to withstand the high temperatures within a fire. The particle size range chosen is a compromise between preferred small particle size to improve flow tracking and large particle size to enhance light scattering (Melling and Whitelaw, 1973). Assuming Stokes flow for particle drag, the response time (time required for particle to reach 63% of the flow velocity) of particles can be estimated using a first-order inertial response to a constant flow acceleration (Raffel et al., 1998).

$$\tau_P = \frac{d_P^2 \rho_P}{18\mu} \tag{1}$$

In Eq. (1), d_p is the diameter of the particle, ρ_P is the density of the particle, and μ is the dynamic viscosity of the fluid. The Al_2O_3 particles have particle response times ranging from 0.4 to 6.4 ms for particle sizes of 10 and 40 μm, respectively, and a refractive index, m, of 1.76. Most of the particles carried into high velocity regions within and above the fire are small to midsize particles, whose time response is closer to 0.4 ms. The response time is in the range of the smallest time between laser pulses and, thus, although not ideal, is reasonable. Based on the viewing area desired (36.0 cm × 27.0 cm), extensive experiments were performed to determine the size of particles that would result in a sufficient amount of scattered light to track the seed particles. Because velocity measurements were also performed within the fire, and the fire also emits light, the chosen particles had to reflect a greater quantity of light than was emitted from the fire to allow for particle tracking. An aerosol generator based on the design by Glass and Kennedy (1977) and adapted by Sun (2006) is utilized to seed the test section. Air at 345 kPa is injected into the aerosol generator, which creates a cloud of particles that are expelled through the top of the aerosol generator. The expelled particles are fed through a seeding pipe (113 cm in length and 1.7 cm in diameter) that is composed of fifty 2 mm diameter, horizontal perforations (25 perforations per side of pipe), ejecting the seed particles horizontally outward. The seed pipe is positioned off center along the length of the fuel bed so that the seed particles are ejected beneath the area of interest, which is in the center of the fuel bed. As the fire front approached the test section, the seed particles were illuminated in a plane at the center of the experimental fuel bed parallel to the direction of fire spread. A double-pulsed Nd: YAG laser (Big Sky Laser Technologies, Inc., model CFR400) located 2 m from the area of interest generated a vertical laser sheet with a wavelength of 532 nm (with energy of 388 mJ/pulse) that illuminated the seed particles. The laser beam was expanded into a 567 mm high and 0.212 mm thick sheet that illuminated seed particles in a vertical plane within the area of interest parallel to the length of the fuel bed. To properly position the waist of the laser sheet, sheet-forming optics, which includes a spherical lens (2000 mm focal length) and a cylindrical lens (15 mm focal length), were used. A LASERPULSE Synchronizer (TSI Inc.) was utilized to trigger the laser pulse and the camera with correct sequences and timing through a 2.66 GHz dual processor workstation (Intel Xeon^{TM}). The laser sheet was synchronized with a high resolution (1600×1192 pixel) POWERVIEW 2 M CCD camera (TSI Inc., model 630157) with a 28 mm f/2.8 Nikkor lens and an exposure time of 260 ms. The camera aperture was set to 11, and a capture rate of 5 image pairs per second (5 Hz) was adopted. The camera was placed 1 m from the area of interest perpendicular to the vertical laser sheet (Figure 1) and set to capture 150 PIV image sets per experiment. The time difference between successive images was optimized for the best PIV quality to $Dt = 400\,\mu s$. This Dt was chosen through experimentation to minimize processing errors obtained when the seed particles, from frame to frame, exit the interrogation regions during PIV data processing. Particle images were captured in a 36.0 cm (horizontal) $\times$ 27.0 cm (vertical) domain. A black background was placed perpendicular to the CCD camera, on the opposite side of the experimental fuel bed, to prevent any light scattering that can introduce background noise in raw images. To reduce the luminosity of the fire and the amount of noise captured by the camera, a

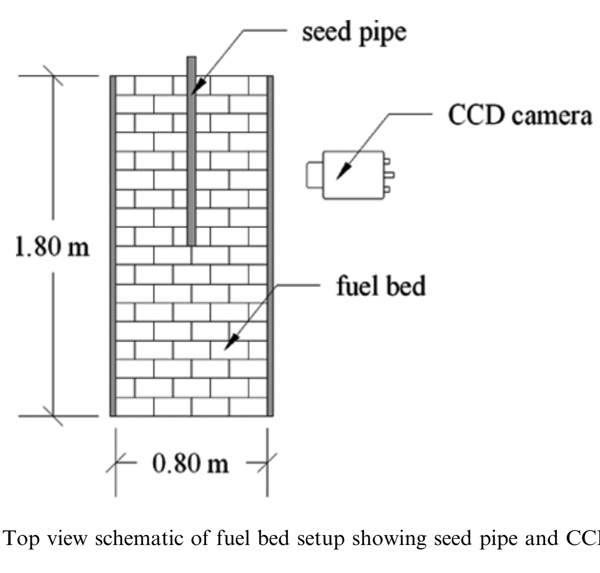

Figure 1 Top view schematic of fuel bed setup showing seed pipe and CCD camera.

532-nm laser line filter was attached to the camera lens. This ensured that only green light (532 nm) was recorded. A grid for PIV processing was formed using a Nyquist Grid engine operating with a 50% overlap over 64×64 pixels interrogation windows resulting in a vector spacing of $3.72\,\text{mm} \times 3.72\,\text{mm}$. Three evaluation passes consisting of a 3×3 median filter to remove spurious vectors was applied to each image. An aluminum meter stick with centimeter marks was used as the calibration object to obtain the geometrical information required to convert pixel to millimeters. Fast Fourier transform correlation was used with the Gaussian peak engine to compute velocities. The velocity fields are obtained using the INSIGHT 3G (version 7.2.0) analysis software. Some instantaneous velocity vector fields contain regions without valid vectors due to the difficulty of homogeneously seeding the region of interest for a single instantaneous PIV image. The out-of-plane vorticity component is computed using second order central differencing of the appropriate velocity components. In order to quantify the size of a coherent vortex, the radius of a coherent vortex structure is defined as the average of the distances from the location of the local peak vorticity magnitude to the points where its magnitude is 20% of the peak value. These distances are measured at increments of 45° starting from 0° to 360°. Twice the average of these distances is calculated and reported as the diameter of the vortex. Utilizing the measured distance, the local vorticity is then determined using $\omega_i = V_{t_i}/r_i$, where ω_i is the local vorticity, r_i is the radius and V_{t_i} is tangential velocity at that location, determined using the PIV velocity data. The average vorticity is then computed using $\bar{\omega} = (1/n)\sum_{i=1}^{n}(V_{t_i}/r_i)$, where $\bar{\omega}$ is the average vorticity, and is henceforth referred to as the vorticity.

2.2. Experimental Setup

Previous analysis has identified nearly 30 dimensionless groups related to fire and explosions (Williams, 2008a) with Reynolds number and Froude number as the most important quantities. Because the focus of the present work is fluid flow in still environment (no induced flow), particularly within the fire, the Froude number is perhaps the most appropriate group to use (Williams, 2008b). The appropriate Froude number is defined as $Fr = U^2/gH$ where U is a characteristic inertial velocity typically measured as wind speed at mid flame height, and H is the characteristic flame height. Froude number scaling maintains balance between convective and gravitational effects during experimentation. Using wind speed data attained from the California State University–San Bernardino virtual weather station, Froude numbers were estimated to range from 0 to 4.8 for a midflame wind speed of 15 m/s and typical flame heights of 5–10 m. In southern California, prescribed burns are performed during marginal burning conditions (Weise et al., 2005) where wind speeds at midflame height are significantly lower than 15 m/s. Midflame wind speeds measured at an elevation of 6.1 m (measured during prescription burning) with an applied wind reduction factor of 0.6 (Rothermel, 1983), are less than 3.3 m/s. The wind reduction factor accounts for the influence of stand and canopy structures on wind. Froude numbers under these conditions are in the range of 0–1.1 according to an estimated flame height of 1.0 m. Accordingly, during experimentation Froude numbers were in the range of 0–1.3 for a midflame wind speed of 2.3 m/s and a characteristic flame height of 40 cm. These experiments were performed at the burn facility located at the USDA Forest Service Forest Fire Laboratory in Riverside, California. The facility is a 13 × 13 m metal building with 6.1 m walls and a vented peaked roof, which is 7.6 m above the concrete floor. Air is introduced at ground level to force smoke up through the roof ventilation system. Aspen (*Populus tremuloides* Michx) excelsior is utilized as a surrogate to represent the surface fuel resulting in a surface fire with a flame height in the range of 0.3–0.5 m. Excelsior is composed of dead wood and its moisture content equilibrates with ambient temperature and relative humidity given sufficient time and steady conditions as most forest surface fuels (Nelson, 2001). Excelsior was chosen because it is cheap, is relatively easy to acquire, burns intensely, and it is relatively easy to prepare a fuel bed with it so that it is homogeneous and the loading is uniform.

The fuel rests on a platform (0.80 m × 1.80 m; Figure 1), comprising alumina firebricks along the bottom and aluminum panels on the sides. These firebricks are employed to decrease the amount of thermal energy absorbed by the fuel bed (thermal conductivity of 3–4 W/m · 8 K). The aluminum panels minimize the amount of radiative energy loss through the sides of the burn bed, thereby allowing the fire front to maintain a nearly linear shape as opposed to a bowed shape. A mass of 0.45 kg of aspen excelsior was evenly distributed over the burn bed to a depth of 0.10 m resulting in a fuel loading of 0.313 kg m^{-2} and a bulk density of 3.13 kg m^{-3}. The packing ratio (bulk density/fuel particle density) of the fuel beds was 0.008. The resulting flame height was safe for indoor experimentation.

Approximately 59 cc of isopropyl alcohol was sprayed on the surface fuel parallel to the width of the fuel (0.80 m) at one end of the fuel bed to ignite the surface fuel in a line ignition. The fuel moisture content was measured using an Arizona Instruments Computrac 1000 moisture analyzer. Accuracy of the moisture analyzer was determined using the Arizona Instruments application data sheet for the Computrac 1000 moisture analyzer. The data sheet contains percent moisture of 64 materials that was determined using the moisture analyzer and oven drying method. From this data the average difference between the moisture measurements from the two methods was approximately 1% with the moisture analyzer giving a moisture reading 1% higher than that attained through the over drying method. A Canon-ZR40 digital camera was used to record each experiment. Instantaneous rate of spread (R), flame tilt angle, and flame height is then determined from the captured images. The instantaneous rate of spread was defined as the distance traversed by a fire in a direction normal to itself per unit time. Flame tilt angle was the angle of the center of the fire from the horizontal and flame height was the average maximum vertical distance between the flame tip and surface fuel (Merrill and Alexander, 1987). The fuel bed setup also allowed for temperature recording using a set of 30 gauge (0.25 mm diameter) type K (Chromel-alumel) thermocouples with a response time of 0.3 s. These thermocouples can be placed anywhere on the surface of the fuel bed.

3. RESULTS

The three regions of a fire were investigated: the continuous flame, intermittent flame, and thermal plume regions. These three regions were investigated because flames encountered in forest fires are generally classified as diffusion flames in which

Table 1 Data for PIV experiments performed in November of 2006 (fuel mass = 450 g; fuel depth = 0.10 m)

Experiment	Ta (°F/°C)	RH %	R (cm/s)	Z_r (cm)	Local time
1	78.1/25.6	46	0.85	16.5	14:40
2	79.1/26.2	45	0.91	16.5	15:10
3	76.7/24.8	52	0.81	16.5	16:20
4	75.4/24.1	53	0.80	16.5	16:43
5	91.9/33.3	17	1.10	16.5	15:23
6	91.9/33.3	17	0.96	16.5	15:54
7	91.4/33.0	16	1.12	16.5	16:01
8	90.5/32.5	16	1.00	16.5	16:15
9	87.7/30.9	19	0.93	40	11:08
10	89.7/32.1	21	0.94	40	11:24
11	89.6/32	27	1.07	40	11:57
12	93.8/34.3	17	1.10	40	12:16
13	96.6/35.9	15	1.11	40	12:39
14	95/65	15	1.12	40	12:58
15	95.8/35.4	20	1.17	8.3	16:05
16	94.2/34.5	16	1.02	8.3	16:24
17	93.1/33.9	20	1.09	8.3	16:46
18	90.3/32.4	19	1.07	8.3	16:54

all three regions exist (Marcelli, 2004). These regions are subsequently defined more precisely. All experiments were conducted under no wind conditions. Ambient air temperature and relative humidity were recorded before each experiment (Table 1).

A total of 18 experiments were performed, although, not all experiments were deemed successful. Some experiments lacked sufficient seed particles to allow for PIV analysis. Other experiments had sufficient seed particles but when analyzed, not enough consecutive velocity vector fields were generated to satisfactorily represent the evolution of the resulting fluid dynamic structures. Each experiment was repeated at least twice for each of the continuous flame, intermittent flame, and thermal plume regions; only a single region was studied in an individual experiment. From all the experiments, the best sequence of images from each region was chosen for discussion and analysis in this paper.

Experiments were conducted over a span of 3 days. Ambient conditions were similar on November 6 and 7, whereas conditions on November 3 were cooler with higher relative humidity (Table 1). These differing ambient conditions resulted in different fuel moistures and a lower rate of spread on November 3. Because of the difference in ambient conditions, the effects of flame region as determined by Z_r, which is the vertical distance from the fuel bed surface to the bottom of the region of interest, are partially confounded with the effects of environmental conditions. The ensuing continuous flame, intermittent flame, and thermal plume regions are distinguished as per Tachajapong (2008). Using the flame height definition and the fact that the flame oscillates with time, three flame regimes can be distinguished. Video images were extracted at 15 frames per second for 7 s. Using these images the minimum and maximum flame heights were determined. The continuous flame region is defined as the distance from the surface fuel to the minimum flame height. The intermittent flame height is defined as the distance from the minimum to the maximum flame height, and beyond the maximum flame height is the thermal plume

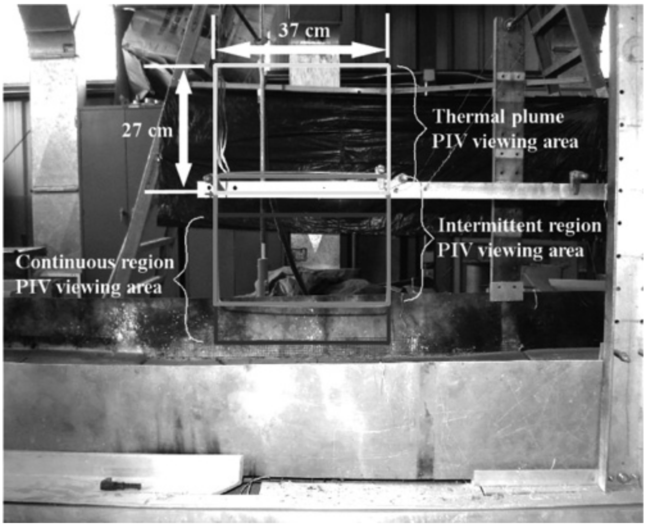

Figure 2 PIV viewing areas for the three fire regimes.

region. The continuous flame, intermittent flame, and thermal plume regions begin at 8.3, 16.5, and 40 cm from the surface fuel, respectively.

The viewing areas captured by the CCD are shown in Figure 2. Here the viewing areas overlap due to the varying size of the three regimes. The continuous flame region is 15 cm in vertical length, followed by the intermittent flame region that ranges from 15 to 45 cm, and the thermal plume region that extends from 45 cm and beyond.

3.1. Continuous Flame Region

In the continuous flame region the vertical component of the velocity magnitude is greatest within the fire column, as was expected. As the surface fuel burns, the hot gaseous products of combustion rise in a column, and because of their higher temperatures and buoyancy, the gaseous products of combustion rise much faster than the surrounding fluid (Groff, 1987; Muñiz and Mungal, 2001; Zukoski et al., 1981). Velocity magnitudes U_m within the flame column range from 0.8 to 2.5 m/s. PIV analysis showed air entrained into the flame from the surroundings with horizontal U_{ent} velocities ranging from 0.4 to 0.5 m/s. Where U_{ent} is the horizontal component of the velocity magnitude U_m of the entrained air. These velocities yield an entrainment coefficient $E = U_{ent}/U_m$ in the range of 0.16–0.63. The higher velocities of the rising gaseous products of combustion and the slower velocities of the entrained air caused a shear at the flame–air interface, resulting in the formation of vortices. The appearance of small and large-scale coherent vortices in instantaneous images is evident in Figures 3a and 3b.

Within the continuous flame region, diameter of vortices ranged from 4.4 to 5.8 cm, shown in Figure 3 (Experiment 16 from Table 1). Although the radiation heat transfer mechanism contributes to preheating unburned fuel ahead of the fire

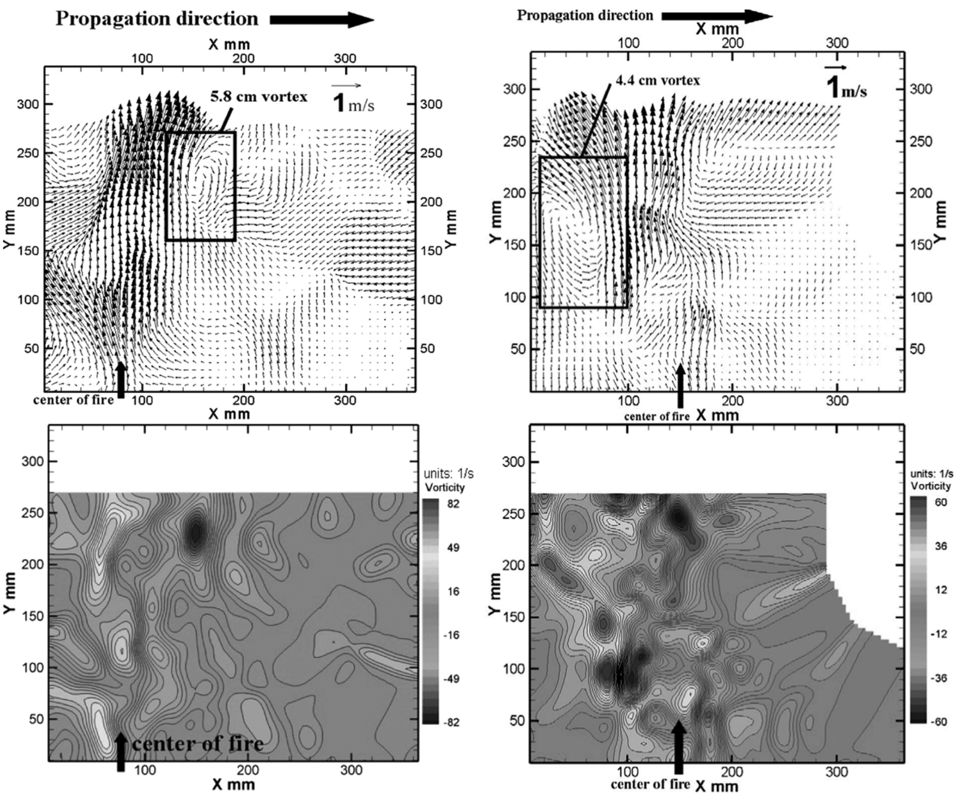

(a) (b)

Figure 3 (a) t = 22 s; Velocity vector field with 5.8 cm diameter vortex on the downwind side and local vorticity contour plot; (b) t = 28 s; velocity vector field showing 4.4 cm diameter vortex on the upwind side and local vorticity contour plot; continuous flame region.

front, convective heating assists preheating at a very short distance downwind of the flame front (Anderson, 1969; Finney et al., 2006; McCarter and Broido, 1965). Figures 3a and 3b show a propagating fire front with a 5.8 cm diameter vortex on the downwind side and a 4.4 cm diameter vortex on the upwind side. Vorticity calculations for the vortices in Figures 3a and 3b result in vorticity values of $17.6\,s^{-1}$ and $15.6\,s^{-1}$ rotating clockwise and counterclockwise, respectively. The vertical arrows at the bottom of the plots indicate the center of the fire front (determined from PIV images where flame is visible) at an instant in time. In Figure 3, top of fuel bed is shown at 0 mm with first velocity vectors calculated 5 mm above fuel bed surface. Sizes of the velocity vectors correspond to the magnitude of the velocity with a vector scale given in the upper right corner.

3.2. Intermittent Flame Region

Analysis of the intermittent flame region shows the formation of vortices and the entrainment of ambient air. Within the intermittent flame region, estimated entrainment velocity U_{ent}, ranged from 0.1 to 0.3 m/s. Within the plume, velocity magnitude U_m, of the hot gaseous products of combustion ranged from 1.0 to 2.1 m/s. These velocities yield an entrainment coefficient E in the range of 0.05–0.3. In the intermittent flame region convective fluid motion does not assist in the preheating of unburned fuel because the fluid does not come in contact with the fuel particles in a still air environment. The largest vortex in this region was approximately 5.8 cm in diameter. Figure 4a (Experiment 4 from Table 1) shows the velocity vector field results for the intermittent flame region with the formation of a 5.8 cm diameter vortex. The vorticity contour plot of Figure 4a is shown in Figure 4b and the vorticity is computed to be $10.3\,s^{-1}$ rotating in the clockwise direction.

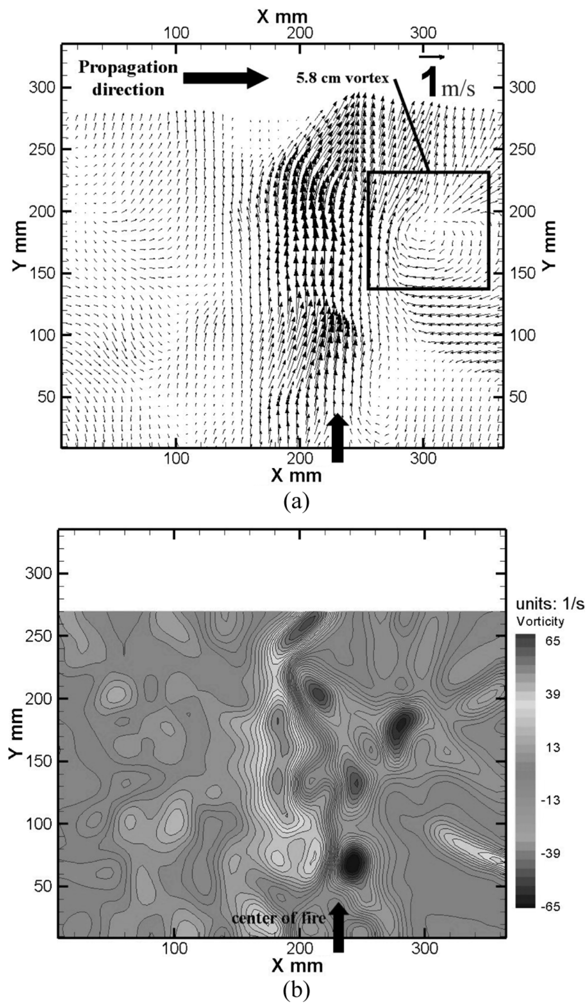

Figure 4 (a) Intermittent flame region image illustrating the formation of a vortex 5.8 cm in diameter; (b) vorticity contour plot showing local vorticity for the image in (a); vortex shown in (a) is rotating at $10.3\,s^{-1}$ clockwise; t = 44 s.

3.3. Thermal Plume Region

Similar observations are made in the analysis of PIV data for the thermal plume region. Within the plume, velocity magnitude of hot gaseous products of combustion ranged from 1.1 to 2.3 m/s. Air is entrained from the surroundings at U_{ent} ranging from 0.1 to 0.3 m/s and has entrainment coefficient E ranging from 0.04 to 0.27. Figures 5a and 5b show the formation of vortices. In the intermittent flame region, Figure 5a (Experiment 4 from Table 1), the vortex is measured to be 3.4 cm in diameter with a vorticity of $10.3\,s^{-1}$. In the thermal plume region, Figure 5b (Experiment 12 from Table 1), the vortex is measured to be 4.6 cm in diameter with a vorticity of $28.8\,s^{-1}$.

Table 2 shows velocity data within the propagating fire for the experiments performed where the continuous flame regions was investigated. Column 1 represents the experiment numbers from Table 1. Columns 2 and 3 contain the average maximum and minimum velocities magnitudes for the three successful continuous

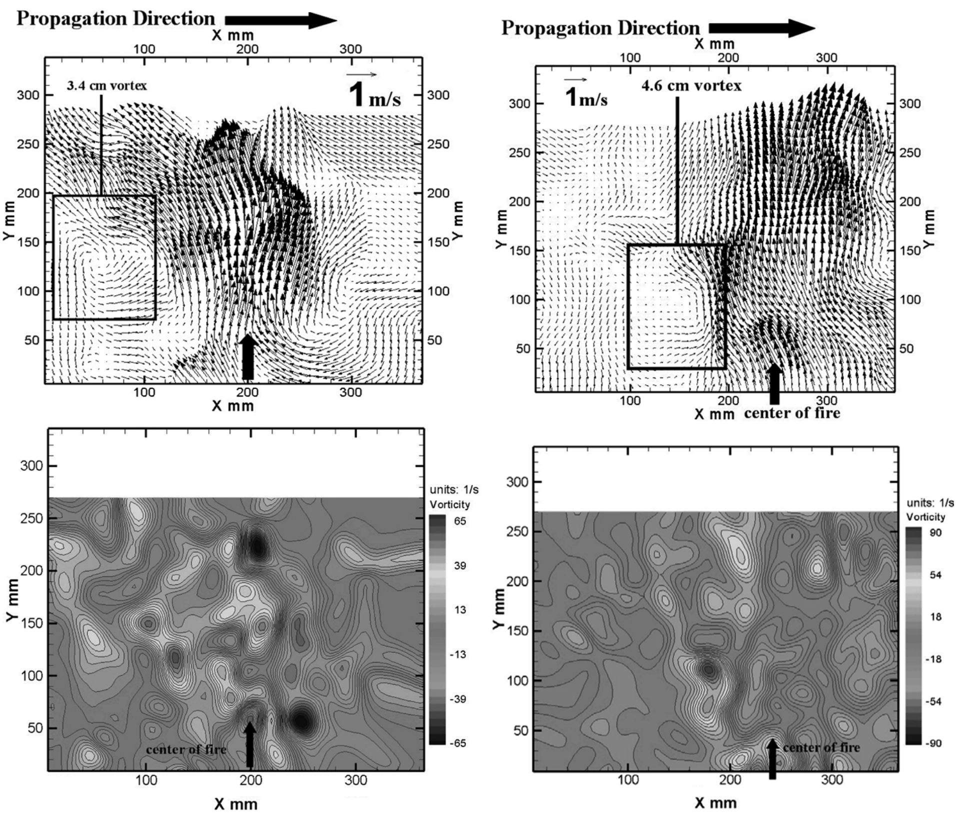

(a) (b)

Figure 5 (a) t = 42 s; Velocity vector field for intermittent flame region showing a 3.4 cm diameter vortex, also shown is the vorticity contour plot used to calculate a vorticity of $10.3\,s^{-1}$; (b) t = 48 s; velocity vector field of thermal plume region showing a 4.6 cm diameter vortex, also shown is the vorticity contour plot used to calculate a vorticity of $28.8\,s^{-1}$.

Table 2 Velocity data for the area within the fire column for the continuous flame region

Experiment	Average maximum velocity (m/s)	Average minimum velocity (m/s)	Average velocity (m/s)
16	2.06	0.019	0.80
17	2.09	0.007	0.69
18	1.18	0.002	0.39

flame region experiments, calculated from the velocity vector fields for each individual experiment. Column 4 represents the average velocity magnitude within the fire column for each experiment.

From the video camera recordings the average rate of spread R was calculated for each experiment by measuring the time the fire required to propagate across the entire fuel bed. Results are shown in Table 1. Using image extraction software and AutoCAD, it was possible to capture the rate of spread history throughout each experiment. Images from video captured during the experiments were extracted every 10 s. The resulting images were then imported into AutoCAD, and the distance the flame traversed every 10 s was measured. Analysis of this data shows that the rate of spread fluctuates as the flame propagates across the fuel bed. A plot of the rate of spread at various positions across the fuel bed for the continuous, intermittent, and thermal regions is shown in Figure 6. The plot shows that initially the flame spreads at a slower rate, and then it accelerates and decelerates as it traverses the fuel bed. The initial low rate of spread is due to the fact that the fuel is line ignited using a small region of fuel at the beginning of the fuel bed, thus resulting in a thin flame that emits a small amount of radiation compared to a thick flame. As the fuel ahead of

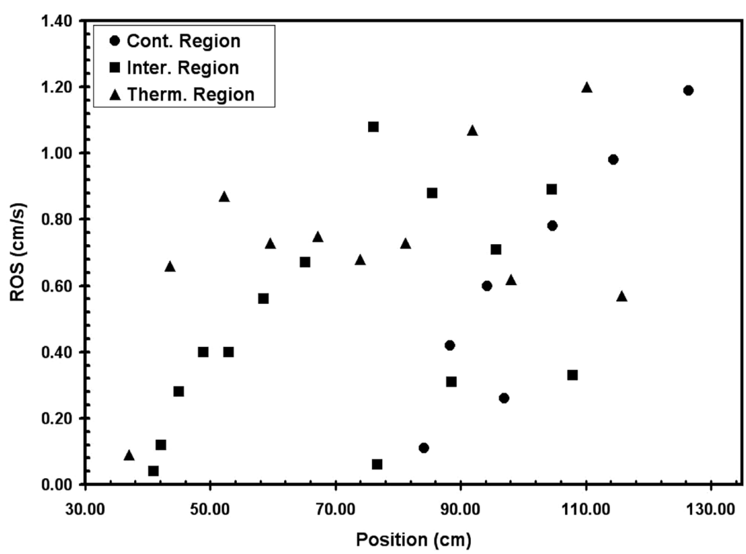

Figure 6 Rate of spread values along the fuel bed for a case of the continuous, intermittent, and thermal regions.

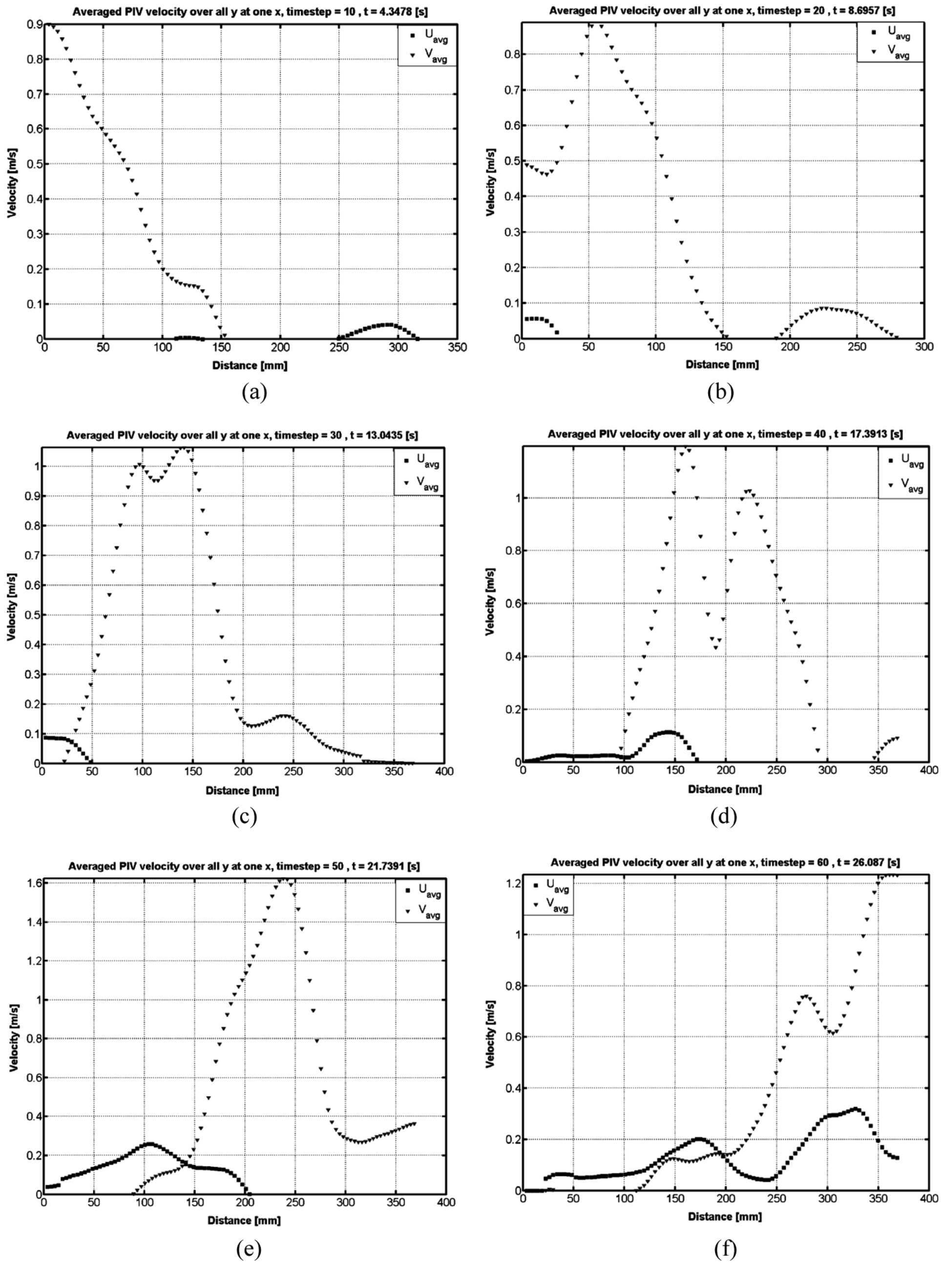

Figure 7 Plots showing the propagation of the fire across the PIV viewing area for a continuous flame region experiment; (a) t = 4.35 s; (b) t = 8.70 s; (c) t = 13.04 s; (d) t = 17.39 s; (e) t = 21.74 s; (f) t = 25.09 s.

the initial fire front ignites, the flame thickness increases. This results in an increased amount of radiation emitted towards the unburned fuel ahead of the fire front and thereby increasing the rate of spread.

Utilizing the PIV data, it is also possible to determine the rate of spread at different locations across the PIV viewing area. The average horizontal, U_x, and vertical, V_y, velocities at every location along the fuel bed were calculated. Peak of the vertical velocity is at the center of the fire, and thus by locating the peak vertical velocity in the generated plots, the fire front center can be tracked approximately as the fire propagates across the PIV viewing area. From the PIV data for a continuous flame region case the R is 1.38, 1.84, 0.26, 1.73, and 2.87 cm/s from Figures 7a–f, respectively. It is apparent that the R values are greater than those attained through analysis of the experiment video images.

From the PIV data it is also possible to visualize the fire center propagation. This is done by plotting the maximum average vertical velocity and minimum horizontal velocity with their positions along the fuel bed, shown in Figure 8. At the fire

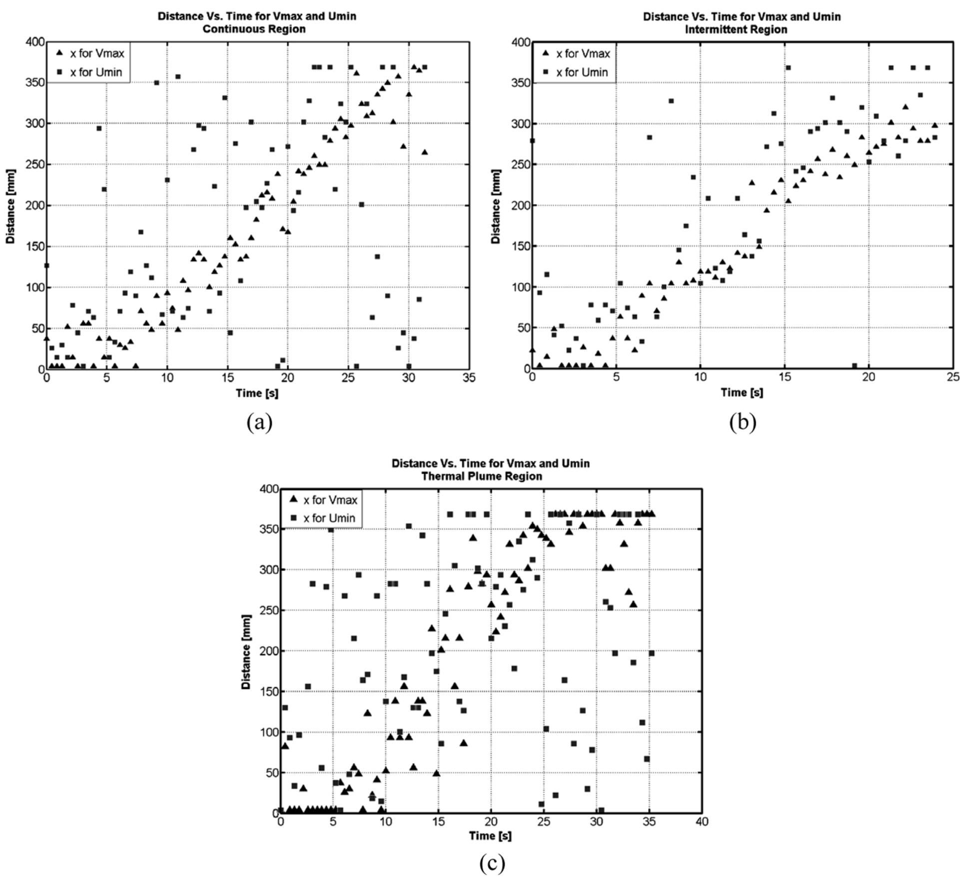

Figure 8 Plot illustrating fire center position over time: (a) continuous flame region; (b) intermittent flame region; (c) thermal plume region.

center the vertical velocity should be maximum and horizontal velocity should be minimum. Accordingly, the two velocities should follow the same trend on the plots. In Figures 8a and 8b it is shown that where vertical velocity is at a maximum then horizontal velocity is at a minimum. Figure 8a (continuous flame region) and 8b (intermittent flame region) show a clearer representation of the fire center movement than does Figure 8c (thermal plume region). Figure 8c shows U_{min} scattered across the plot at areas far from the fire center. This is a result of an increasing plume thickness that assists in distributing the PIV seed particles within the PIV viewing area. The seed particles are no longer concentrated near the fire center, instead they are scattered to areas far from the fire center and thus there is a greater potential for lower velocities outside the fire region as shown in Figure 8c.

4. CONCLUSIONS

Using PIV it was possible to investigate the fluid dynamic structures within the three regions of a flame, and the continuous flame, intermittent flame, and thermal plume regions under no wind conditions. Fire spread across an excelsior bed under no wind conditions is representative of a low intensity fire desired for marginal burning, a condition under which prescribed fires are often carried out. Velocity vector fields in three fire regions and their surrounding were computed. In the continuous flame region, it was determined that the highest velocities, ranging from 0.8 to 2.5 m/s, existed within the fire column as expected. The higher velocities of the gaseous products of combustion and slower velocities of the entrained air caused a shear at the flame-air interface, which resulted in the formation of vortices. It was observed that in the continuous flame region, these vortices ranged from 4.4 to 5.8 cm in diameter. Vortices were observed in all three flame regions. Entrainment coefficients in the continuous flame, intermittent flame, and thermal plume regions were found to be in the ranges of 0.16–0.63, 0.05–0.3, and 0.04–0.27, respectively. Because the vortices are fairly small, it is inferred that under non-wind-aided conditions unburned fuel downstream of the fire front is preheated mainly by radiation from the approaching fire front as opposed to convective preheating from the resulting vortices that contains air at higher temperatures than that of the ambient air.

Sun et al. (2006) correlated mass loss rate, flame height, and heat release rate using pool fire experiments. They observed that maximum flame height was reached a few seconds after ignition and then remained quasi-steady from approximately 30 s for dead chamise fuels and from approximately 45 s for live chamise fuels burned during the spring season. Using dimensionless parameters, introduced by Zukoski (1975) correlating flame height and heat release rate, they established relationships to describe the chamise fire plume. Given that the spread rate in the present experiments are two to three orders magnitude smaller than gas-phase fluid velocities, the fire spread can be considered quasi steady and similar correlations presented by Sun et al. (2006) are likely to be applicable.

To our knowledge, this is the first instance in which such detailed planar velocity field measurements have been made in the vicinity of and within a spreading fire. Further work is required to gain a better understanding of the unsteady flow effects on fire spread. A detailed investigation of the fire dynamics was limited by the relatively low PIV image capture rate of 5 Hz. Sampling at higher rates is important to capture the evolution of the fluid dynamic structures. The next stage is to perform experiments under wind-aided conditions utilizing the PIV system. In these experiments a laboratory scale wind tunnel (1.20 m × 1.20 m × 6.40 m) is used to control wind speed more precisely. To seed the flow field under wind-aided conditions requires a different setup than what was used under non-wind-aided conditions. For these experiments the seed pipe is placed vertically approximately 1 m before the beginning of the fuel bed. As the wind blows, air flow transports seed particle into the vicinity of the fire front, then the particles are entrained into the fire column. It is expected that under the wind-aided conditions stronger, coherent vortices form downstream of the fire front resulting in increased preheating of the unburned fuel, thereby increasing the role of convective heat transfer in the preheating process of unburned fuels. Due to the presence of the wind the combustion rate increases, resulting in higher flow velocities in the vicinity of the fire front and within the fire column. These effects in turn enhance the rate of spread and burning intensity. Direct measurements of velocity can shed light into conditions that could potentially cause spotting in which a fire brand is lofted from the fire, possibly landing in regions containing unburnt fuel. It is expected that by performing a range of experiments spanning no wind to high wind speeds, it would be possible to better understand the dynamics of fire behavior from marginal burning to intense fire spread conditions.

ACKNOWLEDGMENT

This work was made possible through cooperative agreement O6-JV-112 72166-058 with the Forest Fire Laboratory, Pacific Southwest Research Station, USDA Forest Service, Riverside. We are grateful for technical assistance provided by Joey Chong and David Kisor.

REFERENCES

Adrian, R.J. 1988. Review of particle image velocimetry research at the Symposium on Optical Methods in Flow and Particle Diagnostics, 6th International Congress on Application of Lasers and Electro-optics. *Optics and Lasers in Engineering*, **9**, 1561–1576.

Anderson, H.E. 1969. *Heat Transfer and Fire Spread*. USDA Forest Serv. Res. Paper INT-69.

Andrews, P.L. 1986. *BEHAVE: Fire Behavior Prediction System—BURN Subsystem, Part 1*. USDA Forest Serv., Intermountain Res. Sta., Ogden, UT.

Andrews, P.L., and Queen, L.P. 2001. Fire modeling and information system technology. *Inter. J. Wildland Fire*, **10**, 343–352.

Bryant, R.A. 2005. Particle image velocimetry measurements of buoyancy induced flow through a doorway. *NISTIR*, 7252.

Bryant, R.A. 2009a. A comparison of gas velocity measurements in a full-scale enclosure fire. *Fire Safety Journal*, **44**, 793–800.

Bryant, R.A. 2009b. The application of stereoscopic PIV to measure the flow of air into an enclosure containing a fire. *Exp. Fluids*, **47**, 295–308.

Carrier, G.F., Fendell, F.E., and Wolff, M.F. 1991. Wind-aided firespread across arrays of discrete fuel elements. I. Theory. *Combust. Sci. Technol.*, **75**, 31–51.

Catchpole, T., and de Mestre, N. 1986. Physical models for a spreading line fire. *Australian Forestry*, **49**, 102–111.

Clark, T.L., Radke, L., Coen, J., and Middleton, D. 1999. Analysis of small-scale convective dynamics in a crown fire using infrared video camera imagery. *J. Appl. Meteorol.*, **38**, 1401–1420.

Clements, C.B., Zhong, S., Bian, X., Heilman, W.E., and Byun, D.W. 2008. First observations of turbulence generated by grass fires. *J. Geophy. Res.*, **113**.

Cohen, J.D. 1986. *Estimating Fire Behavior with FIRECAST: User's Manual*. USDA Forest Serv. Gen. Techn. Report PSW-90, Berkeley, CA.

Countryman, C.M., and Philpot, C. 1970. *Physical Characteristics of Chamise as a Wildland Fuel*. USDA Forest Serv. Res. Paper PSW-66.

Cruz, M. 2006. Predicting the ignition of crown fuels above a spreading surface fire. Part I: Model idealization. *Inter. J. Wildland Fire*, **15**, 47–60.

Finney, M.A. 1998. *Farsite Users Guide and Technical Documentation*. USDA Forest Serv. Res. Paper RMRS-RP-4.

Finney, M.A., Cohen, J.D., Grenfell, I.C., and Yedinak, K.M. 2006. Experiments on fire spread in discontinuous fuelbeds. *Forest Ecol. Mgmt.*, **234**, S99.

Frandsen, W.H. 1991. Burning rate of smoldering peat. *Northwest Science*, **65**, 166–172.

Glass, M., and Kennedy, I.M. 1977. An improved seeding method for high temperature laser doppler velocimetry. *Combust. Flame*, **29**, 333–335.

Grishin, A.M. 1992. *Matematicheskoye modelirovaniye lesnykh pozharov i novyye sposoby bor'by s nimi* [Mathematical modeling of forest fires and new methods of fighting them]. Novosibirsk, Russia, "Nauka" Publishers, Siberian Division, 408 pp. (Russian).

Groff, E.G. 1987. An experimental evaluation of an entrainment flame-propagation model. *Combustion and Flame*, **67**, 153–162.

Hilbruner, M.W. 1988. Fire behavior modeling for burn prescription specification. Masters Thesis, Colorado State University.

Linn, R., Reisner, J., Colman, J.J., and Winterkamp, J. 2002. Studying wildfire behavior using FIRETEC. *Inter. J. Wildland Fire*, **11**, 233–246.

Long, E., Hargrave, G., Jarvis, S., Justham, T., and Halliwell, N. 2006. Characterization of the interaction between toroidal vortex structures and flame front propagation. *J. Phys.*, Conference Series, **45**, 104–111.

Marcelli, T. 2004. Fire spread across pine needle fuel beds: Characterization of temperature and velocity distributions within the fire plume. *Inter. J. Wildland Fire*, **13**, 37–48.

McCaffrey, J. 1979. Purely buoyant diffusion flames: Some experimental results. *Center for Fire Research, National Engineering Laboratory, National Bureau of Standards*, NBSIR, 79-1910.

McCaffrey, B.J., and Heskestad, G. 1967. Robust bidirectional low-velocity probe for flame and fire application. *Combustion and Flame*, **26**, 125–127.

McCarter, R.J., and Broido, A. 1965. Radiative and convective energy from wood crib fires. *Pyrodynamics*, **2**, 65–85.

Mell, W., Jenkins, M.A., Gould, J., and Cheney, P. 2007. A physics-based approach to modeling grassland fires. *Inter. J. Wildland Fire*, **16**, 1–22.

Melling, A., and Whitelaw, J.H. 1973. Seeding of gas flows for laser anemometry. *DISA Information*, **15**, 5–14.

Meroney, R.N. 2007. Fires in porous media: Natural and urban canopies. In Gayev, Y.A. and Hunt, J.C.R. (Eds.) *Flow and Transport Processes with Complex Obstructions*, NATO Science Series 236. the Netherlands, Springer, pp. 271–310.

Merril, D.F., and Alexander, M.E. 1987. *Glossary of Forest Fire Management Term*, 4th ed., Natl. Res. Counc. Can., Can. Comm. For. Fire Management, Ottawa, Ont. Publ. NRCC No. 26516, p. 91.

Muniz, L., and Mungal, M.G. 2001. Effects of heat release and buoyancy on flow structure and entrainment in turbulent nonpremixed flames. *Combustion and Flame*, **126**, 1402–1420.

Nelson, R.J. 2001. Water relations of forest fuels. In Johnson, E.A. and Miyanishi, K. (Eds.) *Forest Fires: Behavior and Ecological Effects*, Academic Press, San Diego, CA, pp. 79–149.

Ottmar, R.D., Sandberg, D.V., Riccardi C.L., and Prichard, S.J. 2007. An overview of the fuel characteristic classification system—Quantifying, classifying, and creating fuelbeds for resource planning. *Can. J. Forest Res.*, **37**, 2383–2393.

Parsons, R.A. 2006. FUEL3-D: A Spatially Explicit Fractal Fuel Distribution Model. In Andrews, P.L. and Butler, B.W. (Comps.) (Eds.), *Fuels Management—How to Measure Success: Conference Proceedings*, USDA Forest Serv. Proc. RMRS-P-41, Fort Collins, CO, pp. 253–272.

Pastor, E., Zarate, L., Planas, E., and Arnaldos, J. 2003. Mathematical models and calculation systems for wildland fire behavior. *Progress in Energy and Combustion Science*, **29**, 139–153.

Pisaric, M.F.J. 2002. Long-distance transport of terrestrial plant material by convection resulting from forest fire. *Journal of Paleolimnology*, **28**, 349–354.

Pitts, W.M. 1991. Wind effects on fires. *Progress in Energy and Combustion Science*, **17**, 83–134.

Pyne, S.J., Andrews, P.L., and Laven, R.J. 1996. *Introduction to Wildland Fire*, 2nd ed., Wiley, New York.

Raffel, M., Willert, C.E., Werely, S.T., and Kompenhans, J. 1998. *Particle Image Velocimetry: A Practical Guide*, 2nd ed., Springer-Verlag Berlin Heidelberg.

Reuss, D.L., Bardsley, M., Felton, P.G., Landreth, C.C., and Adrian, R.J. 1990. *Velocity, Vorticity, and Strain Rate Ahead of a Flame Measured in an Engine using Particle Image Velocimetry*. SAE Tech. Paper Ser. 900053, SAE Publications Group, Warrendale, PA.

Rothermel, R.C. 1972. A mathematical model for predicting fire spread in wildland fuels. USAA Forest Serv. Res. Paper INT-115.

Rothermel, R.C. 1983. *How to Predict the Spread and Intensity of Forest and Range Fires*, USDA Forest Serv., Intermountain Forest and Range Exp. Sta.

Rothermel, R.C., and Philpot, C.W. 1973. Fire in wildland management: Predicting changes in chaparral flammability. *Journal of Forestry*, **71**, 640–643.

Sun, L. 2006. *Experimental and Theoretical Investigation of Fire Behavior in Live Fuels*. Doctoral dissertation, University of California Riverside, Riverside, CA.

Sun, L., Zhou, X., Mahalingam, S., and Weise, D.R. 2006. Comparison of burning characteristics of live and dead chaparral fuels. *Combustion and Flame*, **144**, 349–359.

Tachajapong, W. 2008. *Understanding Crown Fire Initiation via Experimental and Computational Modeling*. Doctoral dissertation, University of California Riverside, Riverside, CA.

Taylor, S.W., Wotton, B.M., Alexander, M.E., and Dalrymple, G.N. 2004. Variation in wind and crown fire behavior in a northern jack pine-black spruce forest. *Can. J. Forest Res.*, **34**, 1561–1576.

Viegas, D.X. 2004. On the existence of a steady state regime for slope and wind driven fires. *Inter. J. Wildland Fire*, **13**, 101–117.

Weber, R.O. 1991. Modelling fire spread through fuel beds. *Progress in Energy and Combustion Science*, **17**, 67–82.

Weise, D.R., Zhou, X., Sun, L., and Mahalingam, S. 2005. Fire spread in chaparral-'go or no-go'. *Inter. J. Wildland Fires*, **14**, 99–106.

Williams, F.A. 2008a. Mechanistic aspects of the scaling of fires and explosions. In Saito, K. (Ed.), *Progress in Scale Modeling*, the Netherlands, Springer, pp. 29–37.

Williams, F.A. 2008b. Modeling of combustion phenomena. In Saito, K. (Ed.), *Progress in Scale Modeling*, the Netherlands, Springer, pp. 179–195.

Wolff, M.F., Carrier, G.F., and Fendell, F.E. 1991. Wind-aided firespread across arrays of discrete fuel elements. II. Experiment. *Combust. Sci. Technol.*, **77**, 261–289.

Zhou, M., and Garner, C.P. 1995. *Flame Propagation and Laminar Burning Velocity Measurements in a Cylindrical Combustion Chamber using Particle Image Velocimetry*. SAE Tech. Paper Ser. 952458, SAE Publications Group, Warrendale, PA.

Zhou, X., Mahalingam, S., and Weise, D.R. 2005. Modeling of marginal burning state of fire spread in live chaparral shrub fuel bed. *Combustion and Flame*, **143**, 183–198.

Zhou, X., Mahalingam, S., and Weise, D.R. 2007. Experimental study and large eddy simulation of effect of terrain slope on marginal burning in shrub fuel beds. *Proc. Combust. Instit.*, **31**, 2547–2555.

Zukoski, E.E. 1975. *Convective Flows Associated with Room Fires*. Semi Annual Progress Report, National Science Foundation Grant No. GI 31892 × 1, Institute of Technology, Pasadena, CA.

Zukoski, E.E. 1995. Properties of fire plumes. In Cox, G. (Ed.), *Combustion Fundamentals of Fire*, Academic Press, London, pp. 101–215.

Zukoski, E.E., Kubota, T., and Cetegen, B. 1981. Entrainment in fire plumes. *Fire Safety J.*, **3**, 107–121.